# Electronic Spectroscopy of the AlSb Molecule: A Theoretical Study

**Anjan Chattopadhyay and Kalyan Kumar Das***

*Physical Chemistry Section, Department of Chemistry, Jadavpur University, Kolkata 700 032, India*

*Received: February 13, 2003; In Final Form: April 10, 2003*

Relativistic configuration interaction calculations are carried out to study the electronic spectrum of the AlSb molecule. Potential energy curves of 44 electronic states within 6 eV of energy are constructed. Spectroscopic constants ($r_e$, $\omega_e$, $T_e$, $D_e$, $\mu_e$) of the low-lying Λ-S states are computed. The equilibrium bond length and vibrational frequency of the ground state ($X^3\Sigma^-$) of AlSb are estimated to be 2.79 Å and 249 $cm^{-1}$, respectively. Effects of the spin−orbit coupling on the spectroscopic properties and potential energy curves of states that correlate with the lowest two dissociation limits are investigated. The computed dissociation energy of the ground-state spin component ($X^3\Sigma^-_{0^+}$) is 1.44 eV. Transition moments of several electric dipole-allowed and spin-forbidden transitions are computed from CI wave functions. Radiative lifetimes of the low-lying excited states of AlSb at the lowest three vibrational levels ($v' = 0, 1, 2$) are estimated. Transitions from the $3^3\Pi_{0^+}$ component to all lower states with $\Delta\Omega = 0, \pm 1$ are predicted. At $v' = 0$, the $3^3\Pi_{0^+}$ component has a lifetime of about 1.26 μs. The electronic states of AlSb are also compared with those of isovalent AlP, GaAs, GaSb, and InSb molecules.

## I. Introduction

The electronic structure and spectroscopy of small molecules and clusters of group III and V elements have been the subject of numerous experimental and theoretical studies.[1−35] Reliable band structure information has been reported for the simple binary compounds InSb, InAs, GaSb, InP, GaAs, AlSb, and GaP in the solid state. The compounds of these molecules and their ions are well known for their semiconducting properties. Smalley and his group[1−6] did pioneering work on many cluster compounds of group III and V elements. Many other workers have been able to isolate diatomic molecules of these compounds in the gas phase as well as in rare-gas matrices. Lemire et al.[7] studied jet-cooled GaAs by resonant two-photon ionization spectroscopy. Neumark and co-workers[8−13] employed negative ion zero-electron kinetic photodetachment spectroscopic techniques to study these types of compounds. Using the laser-vaporizing method, Li et al.[14] observed infrared absorption spectra of InP, InAs, and InSb molecules. However, no attempts have been made so far to study the electronic spectrum of the AlSb molecule either in the gas phase or in rare-gas matrices.

Complete active space SCF (CASSCF)/CI calculations have been carried out on several neutral and ionic molecules of group III and V elements by Balasubramanian and co-workers.[15−26] These authors have reported a number of electronic states of $Al_nX_m$ (X = P, As) and their positive and negative ions.[21−24,26] However, studies of $Al_nSb_m$ molecules have not been attempted. Meier et al.[27] performed large-scale multireference CI calculations on the low-lying electronic state of the isovalent AlP molecule. Potential energy curves, transition energies, dipole moments, ionization potentials, and dissociation energies of low-lying valence states of AlP have been reported by these authors. Recently,[28−36] ab initio-based large-scale CI calculations on other isovalent molecules—GaP, GaAs, GaSb, InP, InAs, InSb, etc.—have been performed. So far there exist no theoretical or experimental data on the electronic structure and spectroscopic properties of the AlSb molecule. For the first time, we report computational results on the potential energy curves and spectroscopic constants of low-lying electronic states of AlSb. Many dipole-allowed and spin-forbidden transitions are discussed. Radiative lifetimes of the excited states are also estimated. We hope the present results may stimulate experimentalists to study the spectroscopy of AlSb in the near future.

## II. Method of Calculations

The semi-core relativistic effective core potentials (RECP) of Al and Sb are taken from Pacios and Christiansen[37] and LaJohn et al.,[38] respectively, for the present calculations of AlSb. The $3s^23p$ valence electrons of Al and $4d^{10}5s^25p^3$ electrons of Sb are kept in the active space, while the remaining electrons are replaced by these pseudopotentials, which include major relativistic corrections other than the spin−orbit coupling. The primitive Gaussian basis functions (4s4p) of Pacios and Christiansen[37] are augmented with two sets of d-polarization functions of exponents $0.328a_0^{-2}$ and $0.09a_0^{-2}$. Thus, the basis set for the aluminum atom is (4s4p2d). Similarly, the 3s3p4d basis set of the Sb atom, as recommended by LaJohn et al.[38] for the use with RECP, is enhanced by adding two s functions of exponents $0.07a_0^{-2}$ and $0.013a_0^{-2}$, and two sets of p functions of exponents $0.03a_0^{-2}$ and $0.01a_0^{-2}$. The final basis set of Sb becomes (5s5p4d) in the uncontracted form. The exponents of the additional basis for the Sb atom are taken from the work of Alekseyev et al.[39] It is expected that the present basis is sufficient to polarize the 5p orbitals of Sb.

The symmetry-adapted molecular orbitals (MOs), which are used as basis functions for carrying out CI, are obtained from the SCF calculations at each internuclear separation for the $\pi^2\ {}^3\Sigma^-$ state. Using pseudopotentials, the number of valence electrons is reduced to 18, and there are 72 SCF-MOs available for CI calculations. However, preliminary investigations show that $4d^{10}$ electrons do not participate in the Al−Sb bonding, at least in the low-lying electronic states of the molecule. To reduce

* Author to whom correspondence should be addressed. E-mail: ju_daskalyan@hotmail.com; kalyankd@vsnl.net.

10.1021/jp034372g CCC: $25.00 
Published on Web 07/12/2003

**TABLE 1: Correlation between the Λ-S States and Atomic States of AlSb**

| Λ-S states | atomic states Al + Sb | relative energy/cm$^{-1}$ expt[a] | calcd |
|---|---|---|---|
| $^3\Sigma^-$, $^3\Pi$, $^5\Sigma^-$, $^5\Pi$ | $^2P + {}^4S$ | 0 | 0 |
| $^1\Sigma^+$, $^1\Sigma^-$(2), $^1\Pi$(3), $^1\Delta$(2), $^1\Phi$, $^3\Sigma^+$, $^3\Sigma^-$(2), $^3\Pi$(3), $^3\Delta$(2), $^3\Phi$ | $^2P + {}^2D$ | 9 352 | 12 377 |
| $^1\Sigma^+$(2), $^1\Sigma^-$, $^1\Pi$(2), $^1\Delta$, $^3\Sigma^+$(2), $^3\Sigma^-$, $^3\Pi$(2), $^3\Delta$ | $^2P + {}^2P$ | 17 948 | 18 402 |

[a] Moore's table in ref 50; energies are averaged over *j*.

the computational labor without losing much accuracy, we have frozen d-electrons in the CI step. Therefore, the remaining eight active electrons are allowed to excite in the generation of configurations by using the MRDCI package of Buenker and co-workers.[40−45] For the lowest few roots, the MRDCI calculations include 90−200 reference configurations which generate a large number of symmetry-adapted configuration state functions. Eight roots are optimized for singlets and triplets, while four roots of quintets are computed in each spatial symmetry. A configuration selection with a threshold of 2.0 $\mu$hartree reduces the total number of configurations in the CI space below 50 000. Energy extrapolation and Davidson's correction[46,47] provide an estimate of the full CI energy. The AlSb molecule has been kept along the *z*-axis, keeping Al at the origin, and the SCF/MRDCI calculations are carried out in the $C_{2v}$ subgroup of the main group in which the molecule belongs. The sums of the squares of the coefficients of reference configurations for the lowest few roots in the chosen selection threshold remain above 0.90.

The spin−orbit operators of Al and Sb, as derived from the corresponding RECPs, are also taken from Pacios and Christiansen[37] and LaJohn et al.,[38] respectively. All states correlating with the $^2P_u$(Al) + $^4S_u$(Sb) and $^2P_u$(Al) + $^2D_u$(Sb) limits are allowed to mix through the spin−orbit coupling. The Λ-S eigenfunctions are used as the basis for the spin−orbit CI calculations. The estimated full CI energies are placed in the diagonal of the Hamiltonian matrix, whereas off-diagonal matrix elements are obtained by employing pairs of selected CI wave functions with $M_s = S$, and applying spin-projection techniques and the Wigner−Eckert theorem. The sizes of the secular equations of $A_1$, $A_2$, and $B_1$ blocks are 45, 46, and 46, respectively, for some selected roots of the Λ-S symmetries. The details of the spin−orbit treatment may be found elsewhere.[48] Potential energy curves are fitted into polynomials in one-dimensional nuclear Schrödinger equations for numerical solutions.[49] Spectroscopic constants of both Λ-S and Ω symmetries are then estimated from the potential curves. Einstein's spontaneous emission coefficients are calculated from the transition dipole moments and transition energies. The radiative lifetimes of excited states at different vibrational levels are obtained by summing over the Einstein coefficients with all lower-lying levels and inverting.

## III. Results and Discussion

**Potential Energy Curves of Low-Lying Λ-S States.** Two quintets and two triplets of $\Sigma^-$ and $\Pi$ symmetries of AlSb correlate with the lowest dissociation limit, Al($^2P_u$) + Sb($^4S_u$). The second asymptote, Al($^2P_u$) + Sb($^2D_u$), can be reached by 18 Λ-S states of the singlet and triplet multiplicities. Several high-lying singlets and triplets converge with the next dissociation limit, Al($^2P_u$) + Sb($^2P_u$). Experimental energies of the dissociation limits shown in Table 1 are averaged over *j*. The computed relative energy of the second dissociation limit is higher than the observed value by about 3000 cm$^{-1}$. Discrepancies of similar magnitude have also been noted for other group III−V molecules[28−33] at the same level of MRDCI calculations. The energy of the third asymptote, however, is overestimated only by about 500 cm$^{-1}$. All 34 states of the Λ-S symmetries correlating with the lowest three dissociation limits of AlSb are studied. In addition, some higher-lying states of singlet, triplet, and quintet spin multiplicities are reported. The computed potential energy curves of singlets, triplets, and quintets are plotted in Figures 1 and 2.

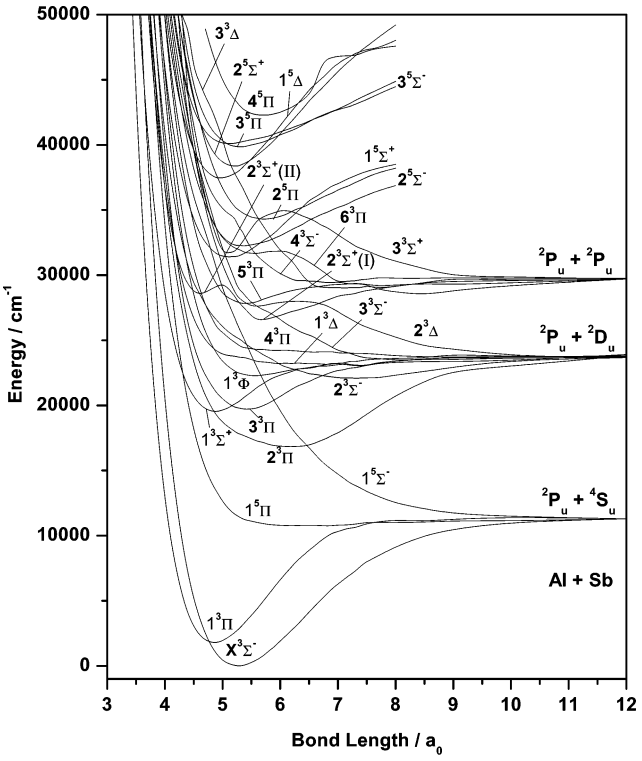


**Figure 1.** Potential energy curves of the triplet and quintet Λ-S states of AlSb.

Table 2 summarizes the spectroscopic parameters ($T_e$, $r_e$, $\omega_e$, $D_e$, and $\mu_e$) of 25 Λ-S states, along with the leading configuration for each state. Like all other group III−V diatomic molecules, the ground-state symmetry of AlSb is $X^3\Sigma^-$. The bond length in the ground state is calculated to be 2.79 Å. The MRDCI-estimated $\omega_e$ of the ground state of AlSb is about 249 cm$^{-1}$. The ground state is described by an open-shell configuration. In the Franck−Condon region, $\sigma$ is mainly a weakly bonding MO comprising s orbitals of Al and Sb. But the contribution of the s(Al) atomic orbital is substantially smaller than that of the s(Sb) orbital. The next $\sigma^*$ orbital is a strongly antibonding combination of s(Al) and s,p$_z$(Sb) atomic orbitals. The third $\sigma$ MO, which is designated as $\sigma'$, is of the strongly bonding type. The s and p$_z$ atomic orbitals of both Al and Sb contribute almost equally in the $\sigma'$ MO. In the equilibrium bond length region, the first occupied $\pi$ MO is purely nonbonding, consisting of p$_{x,y}$ atomic orbitals of Sb. The next $\pi^*$ orbital is, however, antibonding in character. The ground-state configuration also generates $1^1\Delta$ and $2^1\Sigma^+$ states, as shown in Table 3. A closed-shell configuration and an open-shell one of the type $\sigma^{*2}\pi^3\pi^*$ also contribute substantially in the representation of the $2^1\Sigma^+$ state. Energetically, $1^1\Delta$ is located about 5500 cm$^{-1}$ below the $2^1\Sigma^+$ state. The $1^1\Delta$ state dissociates into $^2P_u$(Al) + $^2D_u$(Sb), while $2^1\Sigma^+$ converges with the next higher asymptote. Both $1^1\Delta$ and $2^1\Sigma^+$ states are strongly bound, with estimated binding energies of 2.04 and 2.1 eV, respectively. The $2^1\Sigma^+$

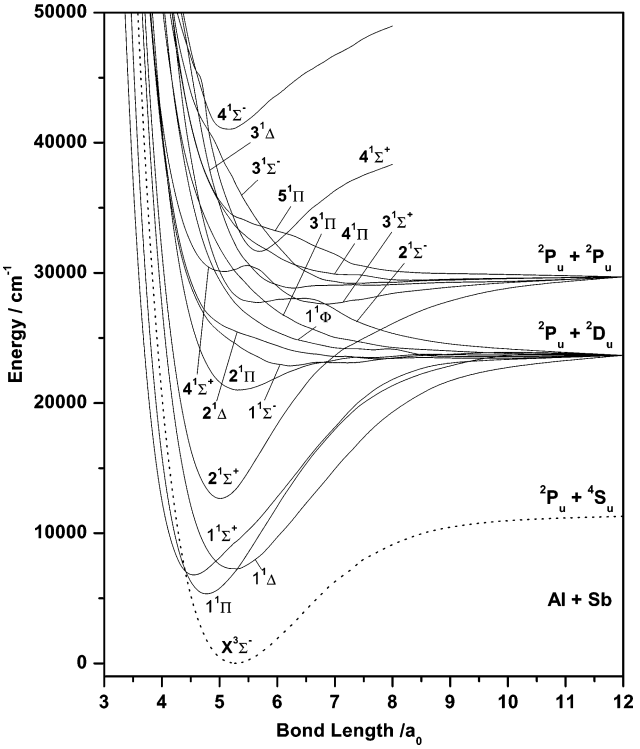


**Figure 2.** Potential energy curves of the singlet Λ-S states of AlSb.

**TABLE 2: Spectroscopic Constants of the Low-Lying Λ-S States of AlSb**

| state | $T_e$/cm$^{-1}$ | $r_e$/Å | $\omega_e$/cm$^{-1}$ | $D_e$/eV | $\mu_e$/D |
|---|---|---|---|---|---|
| $(\sigma'^2\pi^2)$ $X^3\Sigma^-$ | 0 | 2.79 | 249 | 1.40 | −0.98 |
| $(\sigma'\pi^3)$ $1^3\Pi$ | 1 777 | 2.57 | 301 | 1.18 | −1.27 |
| $(\sigma'\pi^3)$ $1^1\Pi$ | 5 296 | 2.53 | 336 | 2.27 | −1.50 |
| $(\pi^4)$ $1^1\Sigma^+$ | 6 805 | 2.42 | 348 | 2.09 | −1.81 |
| $(\sigma'^2\pi^2)$ $1^1\Delta$ | 7 250 | 2.76 | 265 | 2.03 | −0.42 |
| $(\sigma'^2\pi^2)$ $2^1\Sigma^+$ | 12 741 | 2.65 | 348 | 2.12 | −0.13 |
| $(\sigma'\pi^2\pi^*)$ $2^3\Pi$ | 16 865 | 3.25 | 129 | 0.85 | −0.46 |
| $(\pi^3\pi^*)$ $1^3\Sigma^+$ | 19 573 | 2.58 | 265 | 0.52 | −0.25 |
| $(\sigma'\pi^2\pi^*)$ $3^3\Pi$ | 19 753 | 2.86 | 200 | 0.49 | 1.16 |
| $(\sigma'\pi^2\pi^*)$ $2^1\Pi$ | 21 022 | 2.82 | 209 | 0.33 | 0.10 |
| $(\sigma'\pi^2\pi^*)$ $1^3\Phi$ | 22 307 | 2.94 | 153 | 0.17 | |
| $(\sigma'^2\pi\pi^*)$ $2^3\Sigma^+$(I) | 26 573 | 3.03 | 216 | 0.43 | |
| $(\sigma'^2\pi\pi^*)$ $3^1\Sigma^+$ | 27 652 | 3.61 | 119 | 0.26 | |
| $(\sigma'\pi^2\pi^*)$ $5^3\Pi$ | 27 885 | 2.85 | 198 | 0.23 | |
| $(\sigma^*\sigma'\pi^4)$ $2^3\Sigma^+$(II) | 28 591 | 2.44 | 376 | 0.14 | |
| $(\pi^2\pi^{*2})$ $4^1\Sigma^+$ | 30 094 | 2.67 | 231 | | |
| $(\sigma^*\sigma'\pi^3\pi^*)$ $^5\Sigma^+$ | 31 389 | 2.70 | 240 | | |
| $(\sigma'\sigma_5\pi^2)$ $2^5\Sigma^-$ | 32 213 | 2.85 | 208 | | |
| $(\sigma^*\sigma'^2\pi^2\pi^*)$ $2^5\Pi$ | 34 320 | 3.02 | 185 | | |
| $(\sigma^*\sigma'\pi^3\pi^*)$ $1^5\Delta$ | 37 455 | 2.63 | 284 | | |
| $(\pi^2\pi^{*2})$ $2^5\Sigma^+$ | 38 385 | 2.75 | 270 | | |
| $(\sigma'\pi^2\pi_3)$ $3^5\Pi$ | 39 870 | 2.82 | 195 | | |
| $(\sigma^*\sigma'\pi^3\pi^*)$ $3^5\Sigma^-$ | 40 103 | 2.72 | 188 | | |
| $(\sigma'\sigma_5\pi^2)$ $4^1\Sigma^-$ | 41 044 | 2.74 | 300 | | |
| $(\sigma'\pi^2\pi^*)$ $4^5\Pi$ | 42 250 | 3.03 | 215 | | |

**TABLE 3: States Resulting from Low-Lying Configurations**

| configuration | states |
|---|---|
| $\sigma'^2\pi^2$ | $X^3\Sigma^-$, $1^1\Delta$, $2^1\Sigma^+$ |
| $\sigma'\pi^3$ | $1^1\Pi$, $1^3\Pi$ |
| $\pi^4$ | $1^1\Sigma^+$ |
| $\sigma'\pi^2\pi^*$ | $2^1\Pi$, $3^1\Pi$, $4^1\Pi$, $1^1\Phi$, $2^3\Pi$, $3^3\Pi$, $4^3\Pi$, $5^3\Pi$, $1^3\Phi$, $1^5\Pi$ |

state has a shorter bond length and a larger $\omega_e$ as compared with those of $1^1\Delta$. This is mainly due to a strong avoided crossing between the curves of $1^1\Sigma^+$ and $2^1\Sigma^+$ states near $5.3a_0$. Although such a crossing is not evident from the potential curves (Figure 2), the CI coefficients at different bond distances in the curves confirm it. The spectroscopic parameters of these two $^1\Sigma^+$ states in Table 2 are obtained by fitting the adiabatic curves. The $1^1\Sigma^+$ state has the shortest Al−Sb bond length ($r_e$ = 2.42 Å) of all low-lying states reported here. The state has almost the same $\omega_e$ value as in $2^1\Sigma^+$. An open-shell configuration, $\pi^3\pi^*$ ($c^2$ = 0.22), is also important in the representation of $1^1\Sigma^+$ at $r_e$.

The first excited state, $^3\Pi$, which lies only 1777 cm$^{-1}$ above the ground state, is a result of the $\sigma' \rightarrow \pi$ excitation. The $1^3\Pi$ state of AlSb has a bond length ($r_e$ = 2.57 Å) shorter than that of the ground state. The $1^3\Pi$ state is strongly bound, with $\omega_e$ = 301 cm$^{-1}$ and $D_e$ = 1.18 eV. The $1^1\Pi$ state arising from the same excitation as in the triplet counterpart has a transition energy of 5296 cm$^{-1}$. It has an even shorter bond length and a larger vibrational frequency. The $1^1\Pi$ state has a larger binding energy than $1^3\Pi$ because they correlate with different dissociation limits.

The minimum in the potential curve of $2^3\Pi$ is essentially due to a strongly avoided crossing between the curves of the lowest two roots of the $^3\Pi$ symmetry. In the shorter bond length region, the $2^3\Pi$ state is described by $\sigma'\pi^2\pi^*$, while in the longer bond length region, it is dominated by the $\sigma'\pi^3$ configuration. As a result, the estimated equilibrium bond length is much longer ($r_e$=3.25 Å) and the vibrational frequency is considerably small. Hence, the $2^3\Pi$ state does not undergo a strong transition either to the ground state or to the $1^3\Pi$ state. Besides $2^3\Pi$, nine other Λ-S states originate from the same $\sigma' \rightarrow \pi^*$ excitation. The calculations show that the $1^1\Phi$ state is repulsive, while $1^3\Phi$ is weakly bound, with an approximate binding energy of 0.17 eV. The potential minimum of the $1^3\Phi$ state is located around 2.94 Å. Both of these states dissociate into the second asymptote. Of the remaining seven states, the repulsive $1^5\Pi$ state correlates with the lowest dissociation limit. Potential energy curves of three triplets, $3^3\Pi$, $4^3\Pi$, and $5^3\Pi$, and three singlets, such as $2^1\Pi$, $3^1\Pi$, and $4^1\Pi$, are shown in Figures 1 and 2. The $3^3\Pi$ state is bound by about 0.49 eV, and its computed transition energy at equilibrium is 19 753 cm$^{-1}$, with $r_e$ = 2.86 Å and $\omega_e$ = 200 cm$^{-1}$. A reasonably strong $3^3\Pi-X^3\Sigma^-$ transition is expected to take place around 20 000 cm$^{-1}$. The potential curve of the $4^3\Pi$ state is repulsive in nature, while $5^3\Pi$ has a shallow potential minimum, with an estimated transition energy of 27 885 cm$^{-1}$. Of three excited singlet Π states arising out of the $\sigma'\pi^2\pi^*$ configuration, only $2^1\Pi$ is reasonably strongly bound, while $3^1\Pi$ and $4^1\Pi$ states have repulsive potential curves. The equilibrium bond length of the $2^1\Pi$ state is comparable with that of the ground state. The computed transition energy of the $2^1\Pi$ state is about 21 022 cm$^{-1}$. The potential energy curve of the $5^1\Pi$ state is repulsive.

The lowest state of the $^3\Sigma^+$ symmetry lies very close to $3^3\Pi$. However, the $1^3\Sigma^+$ state has a comparatively shorter bond length ($r_e$ = 2.58 Å). The higher excited $^3\Sigma^+$ states have some typical features in their potential curves. Potential energy curves of the second and third roots of the $^3\Sigma^+$ symmetry cross around $5.0a_0$. This has created a double minimum in the adiabatic curve of $2^3\Sigma^+$. The lower energy state, at $r_e$ = 3.03 Å, is denoted by $2^3\Sigma^+$(I), while the higher energy, short-distance minimum is designated as $2^3\Sigma^+$(II). The estimated transition energies of these two states are 26 573 and 28 591 cm$^{-1}$, respectively. At $r_e$, the $2^3\Sigma^+$(II) state has two more configurations in addition to the leading one reported in Table 2. A barrier in the potential curve of $3^3\Sigma^+$ around $r = 6.0a_0$ is due to another avoided crossing with its next higher root.

Potential energy curves of third and fourth roots of $^1\Sigma^+$ undergo an avoided crossing near $5.6a_0$, which is confirmed

from the CI compositions of $3^1\Sigma^+$ and $4^1\Sigma^+$ at various points in the potential curves. The $3^1\Sigma^+$ state has a shallow potential well with a longer equilibrium bond length of 3.61 Å, while the $4^1\Sigma^+$ state has a sharp potential minimum at $r = 2.67$ Å. The diabatic curve of $4^1\Sigma^+$ dissociates into the higher asymptote, while the $3^1\Sigma^+$ state correlates with the third dissociation limit. In the Franck−Condon region, the $4^1\Sigma^+$ state is far more complicated, and several configurations contribute strongly.

Three higher roots of the $^1\Sigma^-$ symmetry are also reported in this study. There is a shallow minimum at 3.0 Å in the potential curve of $2^1\Sigma^-$, and it is bound only by 350 $cm^{-1}$. The avoided crossing with the next higher root around the bond length of $6.5a_0$ forces the $2^1\Sigma^-$ state to predissociate into $^2P_u + {}^2D_u$, while the $3^1\Sigma^-$ state dissociates into the higher asymptote. The $4^1\Sigma^-$ state is strongly bound, but the potential energy curves of $3^1\Sigma^-$ and $4^1\Sigma^-$ undergo avoided crossing near $r = 5.0a_0$. The transition energy, bond length, and vibrational frequency of $4^1\Sigma^-$, estimated from the adiabatic curve, are 41 044 $cm^{-1}$, 2.74 Å, and 300 $cm^{-1}$, respectively. Both $2^1\Delta$ and $3^1\Delta$ states are repulsive in nature.

Besides the repulsive $1^5\Pi$ and $1^5\Sigma^-$ states, there is a bunch of bound excited quintets between 30 000 and 40 000 $cm^{-1}$. The lowest $1^5\Sigma^+$ bound state lies 31 389 $cm^{-1}$ above the ground state. At the equilibrium bond length, the state has a multiconfiguration character, and the leading configuration is shown in Table 2. The computed transition energy of the $2^5\Sigma^+$ state at $r_e = 2.75$ Å is 38 385 $cm^{-1}$, with $\omega_e = 270$ $cm^{-1}$. A strong interaction between the $1^5\Sigma^+$ and $2^5\Sigma^+$ states is predicted. At their respective $r_e$ values, almost the same set of configurations represents both states. However, the $\sigma^*\sigma'\pi^3\pi^*$ configuration dominates in $1^5\Sigma^+$, while the largest contribution in $2^5\Sigma^+$ comes from $\sigma^{*2}\pi^2\pi^{*2}$. In the longer bond length region, the situation is reversed, which justifies the avoided crossing between them. There are two strongly bound excited states of the $^5\Sigma^-$ symmetry. The $2^5\Sigma^-$ state is situated 32 213 $cm^{-1}$ above the ground state, while $3^5\Sigma^-$ has a transition energy of 40 103 $cm^{-1}$. The $r_e$ and $\omega_e$ values of these two states are similar in magnitude. Three high-lying bound states, $2^5\Pi$, $3^5\Pi$, and $4^5\Pi$, have transition energies of 34 320, 39 870, and 42 250 $cm^{-1}$, respectively. The remaining $1^5\Delta$ state is 37 455 $cm^{-1}$ above the ground state. The computed equilibrium bond length of this state is even shorter than the ground-state $r_e$.

The ground-state dissociation energy ($D_e$) of AlSb is 1.40 eV, obtained from the MRDCI calculations at a large bond length without the d-electron correlation and the spin−orbit coupling. At the same level of CI calculations,[32] the $D_e$ value of the heavier GaSb has been reported to be 1.30 eV. Earlier CI calculations by Meier et al.[27] on the isovalent AlP molecule underestimated the ground-state $D_e$ by about 0.34 eV. Although there is no reliable experimental $D_0^0$ value for AlSb, the d-electron correlation, the enhancement of the AO basis size, and the reduction of the configuration selection threshold are expected to increase the dissociation energy to some extent. Moreover, the use of pseudopotentials plays an important role in the computation of dissociation energies.

**Spin−Orbit Coupling and Its Effect on the Spectroscopic Features.** All Λ-S states dissociating into the lowest two limits are allowed to mix through the spin−orbit coupling. The dissociation correlations between the atomic and Ω states of AlSb, corresponding to $Al(^2P_u) + Sb(^4S_u)$ and $Al(^2P_u) + Sb(^2D_u)$, which split into six limits, are shown in Table 4. The computed spin−orbit splitting of the ground state of Al is in the range 175−416 $cm^{-1}$, as compared with the experimental value of 113 $cm^{-1}$. The observed $^2D_{5/2}-{}^2D_{3/2}$ splitting of the Sb atom is 1342 $cm^{-1}$, while the value obtained from the present calculations lies between 1310 and 1500 $cm^{-1}$. Table 4 shows that all four calculated limits arising from $Al(^2P_u) + Sb(^2D_u)$ are higher than the experimental ones by more than 3000 $cm^{-1}$. This is mainly due to the underestimation of the ground-state dissociation energy. Potential energy curves of states with $\Omega = 0^+$, 1, 3 are shown in Figures 3 and 4. Since the components with $\Omega = 0^-$, 2, 4 are not important from the spectroscopic point of view, their potential energy curves are not shown. Spectroscopic parameters of 22 bound states within 25 000 $cm^{-1}$ of energy are given in Table 5. The spin−orbit components of the ground state of AlSb are separated by about 224 $cm^{-1}$, with the $0^+$ component lying below the other component. However, the $r_e$ and $\omega_e$ values of these two components do not differ significantly. The contribution of $1^3\Pi$ in $X^3\Sigma_1^-$ around the equilibrium bond length is somewhat larger than that in the other component. The spin−orbit splitting of the $1^3\Pi$ state takes place in the inverted order. The largest splitting between $1^3\Pi_2$ and $1^3\Pi_{0^-}$ components is about 2389 $cm^{-1}$. These two components remain unperturbed by the spin−orbit mixing, as there are no nearby components with $\Omega = 2$ and $0^-$ for coupling. On the other hand, $1^3\Pi_1$ and $1^3\Pi_{0^+}$ are strongly coupled with the respective components of $X^3\Sigma^-$. As a result, the spectroscopic constants of $1^3\Pi_1$ and $1^3\Pi_{0^+}$ change considerably. Bond lengths of both of the components are reduced by about 0.05 Å. The

**TABLE 4: Dissociation Relation between the Ω States and Atomic States of AlSb**

| Ω state | atomic states Al + Sb | relative energy/$cm^{-1}$ expt[a] | relative energy/$cm^{-1}$ calc |
|---|---|---|---|
| $0^+$, $0^-$, 1(2), 2 | $^2P_{1/2} + {}^4S_{3/2}$ | 0 | 0 |
| $0^+(2)$, $0^-(2)$, 1(3), 2(2), 3 | $^2P_{3/2} + {}^4S_{3/2}$ | 113 | 175 |
| $0^+$, $0^-$, 1(2), 2 | $^2P_{1/2} + {}^2D_{3/2}$ | 8 512 | 11 450 |
| $0^+(2)$, $0^-(2)$, 1(3), 2(2), 3 | $^2P_{3/2} + {}^2D_{3/2}$ | 8 625 | 11 866 |
| $0^+$, $0^-$, 1(2), 2(2), 3 | $^2P_{1/2} + {}^2D_{5/2}$ | 9 854 | 12 946 |
| $0^+(2)$, $0^-(2)$, 1(4), 2(3), 3(2), 4 | $^2P_{3/2} + {}^2D_{5/2}$ | 9 967 | 13 177 |

[a] Reference 50.

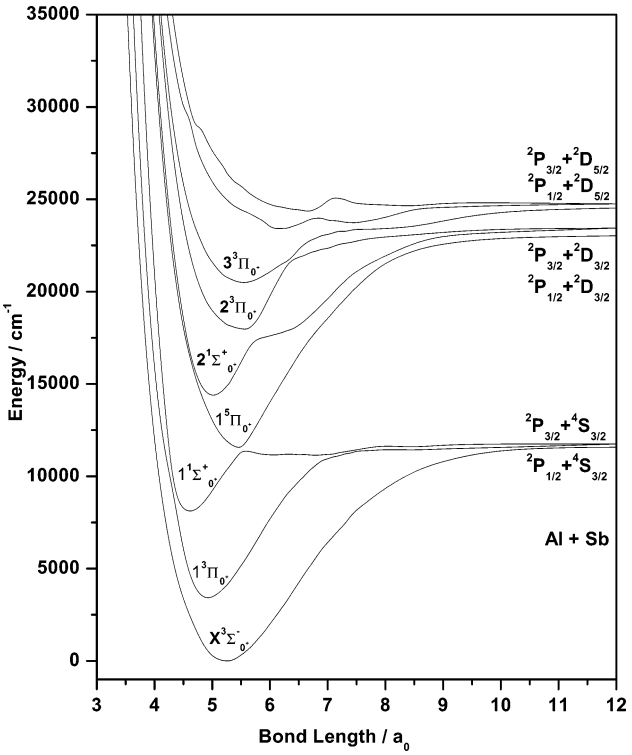


**Figure 3.** Potential energy curves of the low-lying $\Omega = 0^+$ states of AlSb.

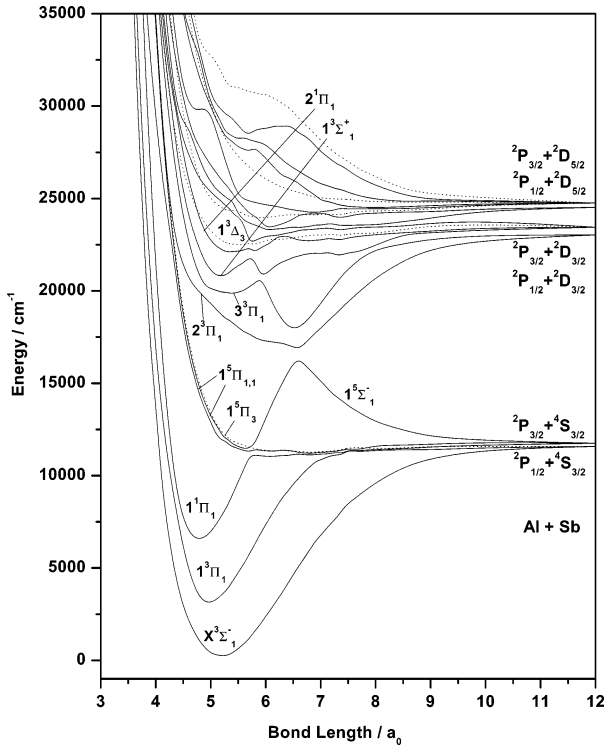


**Figure 4.** Potential energy curves of the low-lying $\Omega = 1$ and $\Omega = 3$ states of AlSb (curves with dashed lines are for $\Omega = 3$).

**TABLE 5: Spectroscopic Constants of the Low-Lying Ω States of AlSb**

| state | $T_e$/cm$^{-1}$ | $r_e$/Å | $\omega_e$/cm$^{-1}$ | composition near $r_e$[a] |
|---|---|---|---|---|
| $X^3\Sigma^-_{0^+}$ | 0 | 2.78 | 232 | $X^3\Sigma^-$(90), $1^3\Pi$(5), $1^1\Sigma^+$(3) |
| $X^3\Sigma^-_1$ | 224 | 2.75 | 222 | $X^3\Sigma^-$(85), $1^3\Pi$(11), $1^1\Pi$(3) |
| $1^3\Pi_2$ | 1 192 | 2.58 | 296 | $1^3\Pi$(96), $1^1\Delta$(4) |
| $1^3\Pi_1$ | 3 127 | 2.64 | 320 | $1^3\Pi$(74), $X^3\Sigma^-$(25), $1^1\Pi$(1) |
| $1^3\Pi_{0^+}$ | 3 375 | 2.62 | 322 | $1^3\Pi$(77), $X^3\Sigma^-$(15), $2^1\Sigma^+$(7) |
| $1^3\Pi_{0^-}$ | 3 581 | 2.58 | 293 | $1^3\Pi$(99) |
| $1^1\Pi_1$ | 6 654 | 2.55 | 312 | $1^1\Pi$(92), $1^3\Pi$(4), $X^3\Sigma^-$(3) |
| $1^1\Sigma^+_{0^+}$ | 8 069 | 2.44 | 355 | $1^1\Sigma^+$(90), $1^3\Pi$(9) |
| $1^1\Delta_2$ | 8 370 | 2.76 | 264 | $1^1\Delta$(94), $1^3\Pi$(6) |
| $2^1\Sigma^+_{0^+}$ | 14 366 | 2.66 | 336 | $2^1\Sigma^+$(91), $1^3\Pi$(5), $X^3\Sigma^-$(3) |
| $2^3\Pi_{0^+}$ | 17 902 | 2.92 | 229 | $2^3\Pi$(80), $2^1\Sigma^+$(12), $3^3\Pi$(2) |
| $3^3\Pi_1$ | 19 881 | 2.84 | 161 | $3^3\Pi$(83), $2^1\Pi$(7), $2^3\Pi$(4), $5^1\Pi$(2) |
| $3^3\Pi_{0^-}$ | 19 982 | 2.74 | 182 | $3^3\Pi$(63), $1^3\Sigma^+$(28), $2^3\Pi$(6) |
| $3^3\Pi_2$ | 20 263 | 2.84 | 211 | $3^3\Pi$(97), $2^3\Delta$(1) |
| $3^3\Pi_{0^+}$ | 20 535 | 2.91 | 183 | $3^3\Pi$(90), $2^3\Pi$(3) |
| $1^3\Sigma^+_1$ | 20 821 | 2.74 | 286 | $1^3\Sigma^+$(67), $2^1\Pi$(13), $3^3\Pi$(7), $2^3\Pi$(5), $2^3\Sigma^-$(3), $4^3\Pi$(2) |
| $2^1\Pi_1$ | 22 105 | 2.86 | 181 | $2^1\Pi$(72), $1^3\Sigma^+$(10), $3^3\Pi$(7), $4^3\Pi$(4), $1^3\Delta$(3) |
| $1^3\Phi_4$ | 23 316 | 2.95 | 152 | $1^3\Phi$(99) |

[a] Numbers in parentheses are percentage contributions.

only component of $1^1\Pi$ is not much perturbed by the spin−orbit coupling. For the next three singlet components, $1^1\Sigma^+_{0^+}$, $1^1\Delta_2$, and $2^1\Sigma^+_{0^+}$, the $r_e$ and $\omega_e$ values remain unchanged, while their transition energies are increased by 1200−1800 cm$^{-1}$. The potential curve of the $1^1\Sigma^+_{0^+}$ component undergoes two avoided crossings, one with $1^3\Pi_{0^+}$ in the shorter bond length region ($\sim 4.5a_0$) and the other with $1^5\Pi_{0^+}$ at the longer bond distance ($\sim 5.7a_0$). The curve of the $2^1\Sigma^+_{0^+}$ component is also subjected to several avoided crossings (Figure 3).

The 2, 1, and $0^-$ components of the repulsive $1^5\Sigma^-$ state play a key role in the interaction with some of the low-lying states. The spin components of the $2^3\Pi$, $1^3\Sigma^+$, and $3^3\Pi$ states are strongly perturbed by the components of $1^5\Sigma^-$. It may be recalled that the potential minimum of $2^3\Pi$ originates from a strongly avoided crossing between the lowest two states of the $^3\Pi$ symmetry. All four components of $2^3\Pi$ get mixed up strongly with other components of the same symmetry. As a result, their potential energy curves become complex in nature. The $2^3\Pi_{0^-}$ state predissociates easily through the repulsive $1^5\Sigma^-_{0^-}$ component. Spectroscopic constants of $2^3\Pi_{0^+}$ are obtained from the adiabatic potential curve. The bond length of $2^3\Pi_{0^+}$ is shortened, while $\omega_e$ is increased considerably as compared with that in the $2^3\Pi$ state. The potential curve of the $3^3\Pi$ state crosses the repulsive curve of $1^5\Sigma^-$ at $6.0a_0$, which is longer than the $r_e$ of $3^3\Pi$ by about $0.6a_0$. Therefore, the spin−orbit components of $1^5\Sigma^-$ perturb the corresponding $3^3\Pi_{2,1,0^-}$ components in the longer bond length region. The $3^3\Pi_{0^+}$ component suffers fewer spin−orbit interactions, and hence survives any predissociation. The compositions of the other three components of $3^3\Pi$ are more complicated. The $3^3\Pi_{0^+}$ component is reasonably strongly bound, and the computed transition energy is around 20 535 cm$^{-1}$. Transitions from $3^3\Pi_{0^+}$ to the low-lying components with $\Delta\Omega = 0, \pm 1$ may be observed experimentally. The spectroscopic constants of all four components of $3^3\Pi$, obtained by fitting the adiabatic potential curves, are given in Table 5. The $r_e$ and $\omega_e$ values of the $3^3\Pi_2$ component are least perturbed. Unlike heavier group III−V molecules, the 2, 1, $0^-$ components of $3^3\Pi$ of AlSb do not predissociate through the interactions with the components of $1^5\Sigma^-$. The $\Omega = 4$ component of $1^3\Phi$ remains unperturbed, as there are no nearby components of the same symmetry for coupling. However, the $1^3\Phi_2$ component is strongly correlated with the neighboring components such as $1^3\Delta_2$, $2^1\Delta_2$, $2^3\Delta_2$ etc. As a result, the $1^3\Phi_2$ component predissociates through the dissociative channel.

**TABLE 6: Radiative Lifetimes (s) of Low-Lying Singlet and Triplet Λ-S States of AlSb[a]**

| transition | lifetime of the upper state $v' = 0$ | $v' = 1$ | $v' = 2$ | total lifetime of upper state at $v' = 0$ |
|---|---|---|---|---|
| $4^1\Sigma^+-1^1\Sigma^+$ | 1.1(−7) | 1.8(−7) | | $\tau(4^1\Sigma^+) = 109(-9)$ |
| $4^1\Sigma^+-2^1\Sigma^+$ | 5.5(−7) | 4.4(−7) | | |
| $4^1\Sigma^+-2^1\Pi$ | 1.56(−5) | 1.63(−5) | 1.73(−5) | |
| $4^1\Sigma^+-1^1\Pi$ | 6.2(−5) | 5.2(−5) | 4.8(−5) | |
| $2^1\Pi-1^1\Delta$ | 6.38(−6) | 6.60(−6) | 6.84(−6) | $\tau(2^1\Pi) = 1.11(-6)$ |
| $2^1\Pi-1^1\Pi$ | 1.36(−6) | 1.41(−6) | 1.69(−6) | |
| $2^1\Pi-1^1\Sigma^+$ | 2.01(−4) | 3.09(−4) | 3.74(−4) | |
| $2^1\Pi-2^1\Sigma^+$ | 2.4(−4) | 2.3(−4) | 2.1(−4) | |
| $2^1\Sigma^+-1^1\Pi$ | 7.97(−6) | 7.97(−6) | 7.96(−6) | $\tau(2^1\Sigma^+) = 6.15(-6)$ |
| $2^1\Sigma^+-1^1\Sigma^+$ | 2.7(−5) | 4.6(−5) | 4.3(−5) | |
| $3^3\Pi$-$X^3\Sigma^-$ | 0.65(−6) | 0.68(−6) | 0.72(−6) | $\tau(3^3\Pi) = 650(-9)$ |
| $3^3\Pi-1^3\Pi$ | 1.54(−4) | 0.38(−4) | 0.19(−4) | |
| $3^3\Pi-2^3\Pi$ | 1.03(−3) | 0.93(−3) | 0.85(−3) | |
| $2^3\Pi$-$X^3\Sigma^-$ | 2.2(−5) | 2.5(−5) | 2.9(−5) | $\tau(2^3\Pi) = 22.0(-6)$ |
| $2^3\Pi-1^3\Pi$ | 85 | 4.6 | 0.5 | |
| $1^3\Sigma^+-1^3\Pi$ | 2.22(−6) | 2.27(−6) | 2.36(−6) | $\tau(1^3\Sigma^+) = 2.22(-6)$ |

[a] Numbers in parentheses are the powers to the base 10.

**Transition Moments, Dipole Moments, and Radiative Lifetimes of Excited States.** Experimentally or theoretically, no electronic transition is known for AlSb. In the absence of any spin−orbit coupling, six triplet−triplet transitions, which originate from the excited $3^3\Pi$, $2^3\Pi$, and $1^3\Sigma^+$ states, are reported here. In addition, several singlet−singlet transitions from $4^1\Sigma^+$, $2^1\Pi$, and $2^1\Sigma^+$ with $\Delta\Lambda = 0, \pm 1$ are also discussed. Table 6 shows partial lifetimes of the upper states at the lowest three vibrational levels involving transitions within 25 000 cm$^{-1}$ of energy.

Among the triplet−triplet transitions, $3^3\Pi-X^3\Sigma^-$ and $3^3\Pi-1^3\Pi$ are expected to take place in the region 18 000−20 000

$cm^{-1}$. The former transition is stronger than the latter. Both the $3^3\Pi-1^3\Pi$ and $3^3\Pi-2^3\Pi$ transitions are comparatively weak. However, the transition dipole moments of these two transitions as a function of the bond length show a smooth behavior. The radiative lifetimes for these two transitions in the lowest vibrational levels are in the order of milliseconds. Summing the transition probabilities of three transitions originating from $3^3\Pi$, the total radiative lifetime of the $3^3\Pi$ state at $v' = 0$ is estimated to be 650 ns. There are two possible transitions from the excited $2^3\Pi$ state. The $2^3\Pi-X^3\Sigma^-$ transition is stronger than the other transition, $2^3\Pi-1^3\Pi$. The Franck−Condon overlap terms for the $2^3\Pi-1^3\Pi$ transition are very small because of a large difference between the $r_e$ values of the $1^3\Pi$ and $2^3\Pi$ states; hence, the transition becomes fairly weak. The computed total radiative lifetime of $2^3\Pi$ is about 22 $\mu$s. The $1^3\Sigma^+-1^3\Pi$ transition is expected to occur around 17 800 $cm^{-1}$, with a computed lifetime of 2.22 $\mu$s at $v' = 0$ for the $1^3\Sigma^+$ state.

Transitions from the $4^1\Sigma^+$, $2^1\Pi$, and $2^1\Sigma^+$ states to the lower-lying singlets are also studied. It is noted that there is a double well in the adiabatic potential curve of the $3^1\Sigma^+$ state due to a strong interaction between the third and fourth roots of the $^1\Sigma^+$ symmetry. The higher-energy potential well holds at least two vibrational levels. So, there is a strong possibility of having four transitions, viz., $4^1\Sigma^+-1^1\Sigma^+$, $4^1\Sigma^+-2^1\Sigma^+$, $4^1\Sigma^+-2^1\Pi$, and $4^1\Sigma^+-1^1\Pi$. At the minimum of $4^1\Sigma^+$, the computed transition moment for the $4^1\Sigma^+-1^1\Sigma^+$ transition is about 0.84 e$a_0$, while that for $4^1\Sigma^+-2^1\Sigma^+$ is nearly half. The estimated partial lifetimes of these two transitions at $v' = 0$, 1 are in the range of 100−600 ns. Other transitions, such as $4^1\Sigma^+-1^1\Pi$ and $4^1\Sigma^+-2^1\Pi$, are comparatively weak. The $4^1\Sigma^+-1^1\Pi$ transition is weaker due to smaller Franck−Condon overlap terms. The radiative lifetime for $4^1\Sigma^+-2^1\Pi$ is 15.6 $\mu$s at $v' = 0$, while that for the $4^1\Sigma^+-1^1\Pi$ transition is nearly 4 times higher. Adding all four transition probabilities, the total radiative lifetime of $4^1\Sigma^+$ at the lowest vibrational is about 109 ns.

Four symmetry-allowed transitions, $2^1\Pi-1^1\Sigma^+$, $2^1\Pi-2^1\Sigma^+$, $2^1\Pi-1^1\Delta$, and $2^1\Pi-1^1\Pi$, involving the $2^1\Pi$ state are possible. The calculations show that the first two transitions are relatively weak. The transition moments of $2^1\Pi-1^1\Sigma^+$ are significantly small throughout the Franck−Condon region. The partial radiative lifetimes at $v' = 0$ for the $2^1\Pi-1^1\Sigma^+$ and $2^1\Pi-2^1\Sigma^+$ transitions are 201 and 240 $\mu$s, respectively. Both the $2^1\Pi-1^1\Pi$ and $2^1\Pi-1^1\Delta$ transitions are expected to have considerable intensities. The partial lifetimes of these two transitions are in the range of 1−7 $\mu$s at the lowest few vibrational levels. The computed total radiative lifetime of the $2^1\Pi$ state at $v' = 0$ is about 1.11 $\mu$s. Two dipole-allowed transitions from the $2^1\Sigma^+$ state are also reported here. The transition moment of the $2^1\Sigma^+-1^1\Sigma^+$ transition shows a maximum around $r = 5.0a_0$, and it falls rapidly with the increase in $r$. The transition moment of the $2^1\Sigma^+-1^1\Pi$ transition varies slowly, and the transition is somewhat stronger than $2^1\Sigma^+-1^1\Sigma^+$. The total lifetime of $2^1\Sigma^+$ is calculated to be 6.15 $\mu$s.

Although many transitions with $\Delta\Omega = 0, \pm1$ are possible, we have focused only on the transitions from the $3^3\Pi_{0^+}$ component as it is less perturbed by the nearby components. Seven transitions from $3^3\Pi_{0^+}$ to the lower states, with $\Omega = 0^+$ and 1, are shown in Table 7. It is noted that the $3^3\Pi_{0^+}-X^3\Sigma^-_{0^+}$ transition is at least 10 times weaker than $3^3\Pi_{0^+}-X^3\Sigma^-_1$. This is mainly due to the presence of a larger $1^3\Pi$ component in $X^3\Sigma^-_1$. Transition dipole moments of both $3^3\Pi_{0^+}-1^3\Pi_{0^+}$ and $3^3\Pi_{0^+}-1^3\Pi_1$ transitions are rapidly varying functions of the bond length. The former transition is somewhat weaker than the latter. Three spin-forbidden transitions, namely, $3^3\Pi_{0^+}-1^1\Sigma^+_{0^+}$, $3^3\Pi_{0^+}-1^1\Pi_1$, and $3^3\Pi_{0^+}-2^1\Sigma^+_{0^+}$, are also studied here. The partial radiative lifetimes of these transitions are of the order of milliseconds. The total lifetime of the $3^3\Pi_{0^+}$ component at $v' = 0$ is about 1.26 $\mu$s.

**TABLE 7: Radiative Lifetime (s) of the $3^3\Pi_{0^+}$ State of AlSb[a]**

| transition | lifetime of the upper state $v' = 0$ | $v' = 1$ | $v' = 2$ | total lifetime of upper state at $v' = 0$ |
|---|---|---|---|---|
| $3^3\Pi_{0^+}-X^3\Sigma^-_{0^+}$ | 1.15(−5) | 1.21(−5) | 1.30(−5) | $\tau(3^3\Pi_{0^+}) = 1.26(-6)$ |
| $3^3\Pi_{0^+}-X^3\Sigma^-_1$ | 1.47(−6) | 2.26(−6) | 3.04(−6) | |
| $3^3\Pi_{0^+}-1^3\Pi_{0^+}$ | 4.99(−5) | 1.49(−5) | 0.93(−5) | |
| $3^3\Pi_{0^+}-1^3\Pi_1$ | 3.20(−3) | 0.55(−3) | 0.18(−3) | |
| $3^3\Pi_{0^+}-1^1\Sigma^+_{0^+}$ | 1.34(−3) | 0.65(−3) | 0.45(−3) | |
| $3^3\Pi_{0^+}-1^1\Pi_1$ | 4.95(−3) | 1.77(−3) | 1.23(−3) | |
| $3^3\Pi_{0^+}-2^1\Sigma^+_{0^+}$ | 4.60(−4) | 4.75(−4) | 4.82(−4) | |

[a] Numbers in parentheses are the powers to the base 10.

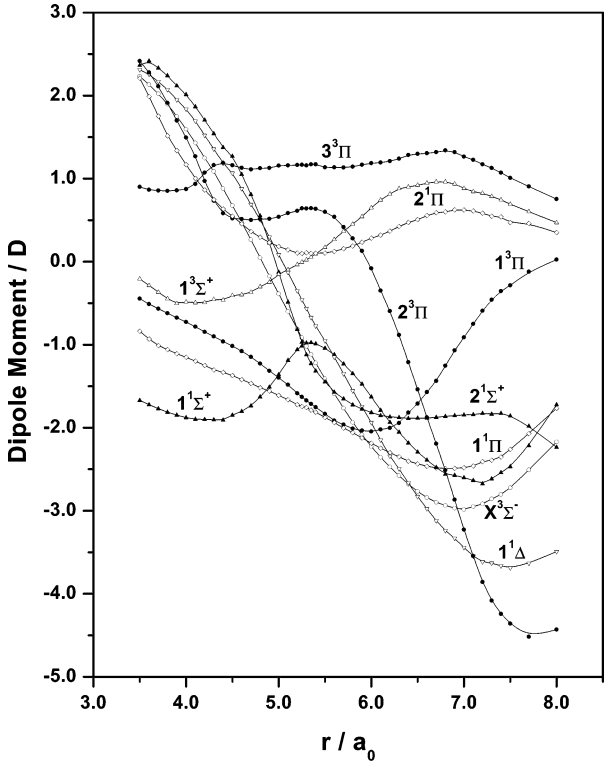


**Figure 5.** Dipole moment functions of 10 low-lying states of AlSb.

Dipole moment functions of at least teh 10 lowest Λ-S states of AlSb are shown in Figure 5. The ground-state $\mu_e$ is estimated to be −0.98 D, where the negative sign refers to the $Al^+-Sb^-$ polarity. The $3^3\Pi$ state has a positive dipole moment throughout the curve, indicating the opposite polarity. At $r_e$, the dipole moment of the $3^3\Pi$ state is 1.16 D. It may be recalled that the $3^3\Pi$ state arises from the $\sigma'\pi^2\pi^*$ configuration in which the $\pi^*$ MO is localized more strongly on the Al atom. So, the electron density is shifted toward Al, and it changes the dipole polarity of the molecule in the $3^3\Pi$ state. The dipole moment of the ground state is maximum (−3 D) near the bond length of $7.0a_0$. The dipole moment curves of $1^1\Pi$, $1^1\Delta$, $1^1\Sigma^+$, and $2^3\Pi$ states have identical patterns in the longer bond length region. The dipole moment of the $2^3\Pi$ state changes very sharply in the region of $5.5-7.5a_0$, and at $r_e$ the value is −0.46 D. Both the $1^3\Pi$ and $1^1\Pi$ states have somewhat larger negative $\mu_e$. The dipole moments of $1^3\Sigma^+$ and $2^1\Pi$ are, however, slowly varying functions.

**Comparison with Isovalent Molecules.** The electronic spectra of the antimonides of Al, Ga, and In, and smaller

**TABLE 8: Comparison of the Computed Spectroscopic Parameters of Isovalent Molecules**

| property[a] | AlP[b] | GaAs[c] | AlSb | GaSb[d] | InSb[e] |
|---|---|---|---|---|---|
| $r_e(X^3\Sigma^-)$, Å | 2.45 | 2.67 | 2.79 | 2.82 | 3.02 |
| $\omega_e(X^3\Sigma^-)$, $cm^{-1}$ | 359 | 179 | 249 | 161 | 139 |
| $D_e(X^3\Sigma^-)$, eV | 1.88 | 1.30 | 1.40 | 1.30 | 1.22 |
| $T_e(1^3\Pi)$, $cm^{-1}$ | 887 | 1 066 | 1 777 | 1 573 | 2 654 |
| $r_e(1^3\Pi)$, Å | 2.26 | 2.39 | 2.57 | 2.57 | 2.81 |
| $\Delta E(1^1\Pi-1^3\Pi)$, $cm^{-1}$ | 3 468 | 4 875 | 3 519 | 4 394 | 4 351 |
| $T_e(1^1\Sigma^+)$, $cm^{-1}$ | 5 404 | 6 690 | 6 805 | 7 450 | 9 002 |
| $r_e(1^1\Sigma^+)$, Å | 2.12 | 2.21 | 2.42 | 2.41 | 2.70 |
| $T_e(3^3\Pi)$, $cm^{-1}$ | 21 857 | 22 250 | 19 753 | 21 508 | 20 108 |
| $r_e(3^3\Pi)$, Å | 2.54 | 2.72 | 2.86 | 2.90 | 3.07 |
| $\omega_e(3^3\Pi)$, $cm^{-1}$ | 213 | 135 | 200 | 113 | 111 |
| zfs, $cm^{-1}$ [f] | | 76 | 224 | 218 | 429 |
| $T_e(3^3\Pi_{0^+})$, $cm^{-1}$ | | 22 178 | 20 535 | 21 771 | 20 094 |
| $r_e(3^3\Pi_{0^+})$, Å | | 2.76 | 2.91 | 3.03 | 3.16 |
| $\omega_e(3^3\Pi_{0^+})$, $cm^{-1}$ | | 125 | 183 | 89 | 102 |
| $\tau_{3^3\Pi_{0^+}}$, $\mu$s | | 1.05 | 1.26 | 1.93 | 2.50 |

[a] The subscript e refers to the parameter at $r_e$ of the corresponding state. [b] Reference 27. [c] Reference 28. [d] Reference 32. [e] Reference 31. [f] Zero field splitting $[^3\Sigma^-(X_21) - {}^3\Sigma^-(X_10^+)]$.

isovalent molecules AlP, GaAs, etc., are very similar. The GaAs molecule has been experimentally well-studied. For others, only ground-state dissociation energies are known. However, a series of theoretical calculations on these molecules at the MRDCI level has been performed in recent years.[27−32] In Table 8, we have compared some important spectroscopic constants of these isovalent molecules. The equilibrium bond length increases and the vibrational frequency decreases from AlSb to InSb due to the increase in mass. The lighter molecule AlP has a shortest bond length. In general, the ground state of the heavier molecule is expected to have a smaller dissociation energy. The calculations show the correct trend of the ground-state dissociation energies of these molecules. The computed $\Delta E(1^1\Pi-1^3\Pi)$ splittings of GaSb and InSb are comparable in magnitude, while the lighter AlSb molecule has a somewhat smaller splitting of 3519 $cm^{-1}$. A greater stability of the $1^3\Pi$ state is noted in GaAs. The equilibrium bond length of the $1^3\Pi$ state is always shorter than the ground-state $r_e$ by 0.20−0.28 Å. The closed-shell $1^1\Sigma^+$ state has the shortest bond length of all the low-lying states of these molecules. The $1^3\Pi$ state is far more stable than $1^1\Sigma^+$, and the relative stability increases with the mass of the molecule. The heavier InSb molecule has the largest $1^1\Sigma^+-1^3\Pi$ energy separation. A strong interaction between $1^1\Sigma^+$ and $2^1\Sigma^+$ is noted in all the isovalent molecules compared here. The energy gap between the second and third roots of $^1\Sigma^+$ is sufficiently large that no mixing between them takes place. The avoided crossing between the curves of the third and fourth roots of the $^1\Sigma^+$ symmetry is a common feature for these molecules. The shapes of the potential curves of $3^1\Sigma^+$ and $4^1\Sigma^+$ states are also quite similar. The $4^1\Sigma^+$ state is strongly bound for all of these molecules.

A broad potential well of the $2^3\Pi$ state with a longer equilibrium bond length looks very similar for these molecules. The well is obtained because of the interaction between a strongly bound $1^3\Pi$ state with its next higher repulsive root. The $3^3\Pi$ state is located in the energy range 19 500−22 250 $cm^{-1}$ for all of these molecules. The $3^3\Pi-X^3\Sigma^-$ band in GaAs has been experimentally observed, and the $3^3\Pi$ state is denoted as $A^3\Pi$. The same band is expected to be observed for other molecules. The computed partial lifetimes for this transition in GaAs, AlSb, GaSb, and InSb molecules are 440, 650, 563, and 530 ns, respectively. The repulsive $1^5\Sigma^-$ state plays a key role in the predissociations of some of the spin−orbit components of the excited $\Pi$ states. The potential curves of both $2^3\Pi$ and $3^3\Pi$ cross the curve of the $1^5\Sigma^-$ state identically. In some cases, the $0^-$, 1, and 2 components of $3^3\Pi$ may predissociate. However, due to the shorter $r_e$ of the $3^3\Pi$ state in AlSb, the avoided crossing takes place at the longer bond distance, which prevents the predissociations of these spin components from occurring. The $3^3\Pi_{0^+}$ components of these molecules undergo many spin-forbidden transitions to the lower $0^+$ and 1 components. The MRDCI-estimated total lifetimes of $3^3\Pi_{0^+}$ at $v' = 0$ are 1.05, 1.26, 1.96, and 2.5 $\mu$s for the respective GaAs, AlSb, GaSb, and InSb molecules. The same for AlP has not been computed so far.

## IV. Summary and Conclusion

Ab initio-based multireference CI calculations using pseudopotentials have demonstrated, for the first time, the electronic spectrum of the AlSb molecule within 45 000 $cm^{-1}$. At least 25 bound states of the $\Lambda$-S symmetry have been reported. The computed $r_e$ and $\omega_e$ values of the ground-state molecule are 2.79 Å and 249 $cm^{-1}$, respectively. There are several excited quintets which sometimes play a key role in changing the chracteristics of the low-lying bound states through the spin−orbit coupling. A strong interaction between the lowest two $^1\Sigma^+$ states of the AlSb molecule increases the vibrational frequency of the $2^1\Sigma^+$ state. An avoided crossing between the potential curves of $3^1\Sigma^+$ and $4^1\Sigma^+$ results in a double minimum. The $4^1\Sigma^+$ state is short-lived, and several symmetry-allowed transitions are expected to take place from it. The broad potential minimum of the $2^3\Pi$ state is due to the interaction between a strongly bound $1^3\Pi$ state and the next repulsive root of the same symmetry. The $3^3\Pi$ state is important from the spectroscopic point of view, as the $3^3\Pi-X^3\Sigma^-$ transition is found to be very strong. The $3^3\Pi$ state is also short-lived, with a lifetime of about 650 ns. The ground-state AlSb molecule has a $Al^+Sb^-$ polarity with $\mu_e = -0.98$ D. The ground-state molecule dissociates into $^2P_u + {}^4S_u$, with a dissociation energy of 1.40 eV.

The zero-field splitting of the ground state of AlSb is only 224 $cm^{-1}$, with the $X^3\Sigma^-_{0^+}$ component lying lower than $X^3\Sigma^-_1$. The $1^3\Pi$ state splits in the inverse order due to the spin−orbit coupling. The largest spin−orbit splitting in $1^3\Pi$ is about 2400 $cm^{-1}$. The interactions of 2, 1, $0^-$ components of both $2^3\Pi$ and $3^3\Pi$ with the corresponding components of the repulsive $1^5\Sigma^-$ state make the potential curves rather complicated. Some of these components predissociate through different dissociative channels. The $3^3\Pi_{0^+}$ component undergoes several strong transitions to the low-lying $0^+$ and 1 components. The computed radiative lifetime of $3^3\Pi_{0^+}$ at $v' = 0$ is about 1.26 $\mu$s.

**Acknowledgment.** The authors are grateful to Prof. Dr. R. J. Buenker, Germany, for allowing us to use his CI codes.

## References and Notes

(1) O'Brien, S. C.; Liu, Y.; Zhang, Q.; Heath, J. R.; Tittel, F. K.; Curl, R. F.; Smalley, R. E. *J. Chem. Phys.* **1986**, *84*, 4074.

(2) Liu, Y.; Zhang, Q.; Tittel, F. K.; Curl, R. F.; Smalley, R. E. *J. Chem. Phys.* **1986**, *85*, 7434.

(3) Zhang, Q.; Liu, Y.; Curl, R. F.; Tittel, F. K.; Smalley, R. E. *J. Chem. Phys.* **1988**, *88*, 1670.

(4) Wang, L.; Chibante, L. P. F.; Tittel, F. K.; Curl, R. F.; Smalley, R. E. *Chem. Phys. Lett.* **1990**, *172*, 335.

(5) Jin, C.; Taylor, K.; Conciecao, J.; Smalley, R. E. *Chem. Phys. Lett.* **1990**, *175*, 17.

(6) Lou, L.; Wang, L.; Chibante, L. P. F.; Laaksonen, R. T.; Nordlanden, P.; Smalley, R. E. *J. Chem. Phys.* **1991**, *94*, 8015.

(7) Lemire, G. W.; Bishea, G. A.; Heidecke, S. A.; Morse, M. D. *J. Chem. Phys.* **1990**, *92*, 121.

(8) Arnold, C. C.; Neumark, D. M. *J. Chem. Phys.* **1994**, *99*, 3353.

(9) Arnold, C. C.; Neumark, D. M. *J. Chem. Phys.* **1994**, *100*, 1797.

(10) Xu, C.; deBeer, E.; Arnold, D. W.; Arnold, C. C.; Neumark, D. M. *J. Chem. Phys.* **1994**, *101*, 5406.
(11) Arnold, C. C.; Neumark, D. M. *Can. J. Phys.* **1994**, *72*, 1322.
(12) Burton, G. R.; Xu, C.; Arnold, C. C.; Neumark, D. M. *J. Chem. Phys.* **1996**, *104*, 2757.
(13) Gómez, H.; Taylor, T. R.; Neumark, D. M. *J. Phys. Chem. A* **2001**, *105*, 6886.
(14) Li, S.; Van Zee, R. J.; Weltner, W., Jr. *J. Phys. Chem.* **1994**, *98*, 2275.
(15) Balasubramanian, K. *Relativistic Effects in Chemistry Part A. Theory and Techniques*; Wiley-Intersciences: New York, 1997.
(16) Balasubramanian, K. *Relativistic Effects in Chemistry Part B. Applications to Molecules and Clusters*; Wiley-Intersciences, New York, 1997.
(17) Feng, P. Y.; Balasubramanian, K. *Chem. Phys. Lett.* **1997**, *265*, 41.
(18) Feng, P. Y.; Balasubramanian, K. *Chem. Phys. Lett.* **1997**, *265*, 547.
(19) Feng, P. Y.; Balasubramanian, K. *Chem. Phys. Lett.* **1998**, *283*, 167.
(20) Feng, P. Y.; Balasubramanian, K. *Chem. Phys. Lett.* **1998**, *284*, 313.
(21) Feng, P. Y.; Balasubramanian, K. *Chem. Phys. Lett.* **1999**, *301*, 458.
(22) Feng, P. Y.; Balasubramanian, K. *J. Phys. Chem. A* **1999**, *103*, 9093.
(23) Feng, P. Y.; Balasubramanian, K. *Chem. Phys. Lett.* **2000**, *318*, 417.
(24) Feng, P. Y.; Balasubramanian, K. *J. Phys. Chem. A* **2001**, *105*, 11295.
(25) Feng, P. Y.; Balasubramanian, K. *J. Phys. Chem. A* **2000**, *104*, 1969.
(26) Feng, P. Y.; Dai, D.; Balasubramanian, K. *J. Phys. Chem. A* **2000**, *104*, 422.
(27) Meier, U.; Peyerimhoff, S. D.; Bruna, P. J.; Karna, S. P.; Grein, F. *Chem. Phys.* **1989**, *130*, 31.
(28) Manna, B.; Das, K. K. *J. Phys. Chem. A* **1998**, *102*, 9876.
(29) Manna, B.; Das, K. K. *J. Mol. Struct. (THEOCHEM)* **1999**, *467*, 135.
(30) Manna, B.; Dutta, A.; Das, K. K. *J. Phys. Chem. A* **2000**, *104*, 2764.
(31) Manna, B.; Dutta, A.; Das, K. K. *J. Mol. Struct. (THEOCHEM)* **2000**, *497*, 123.
(32) Dutta, A.; Chattopadhyay, A.; Das, K. K. *J. Phys. Chem. A* **2000**, *104*, 9777.
(33) Dutta, A.; Giri, D.; Das, K. K. *J. Phys. Chem. A* **2001**, *105*, 9049.
(34) Balasubramanian, K. *J. Chem. Phys.* **1987**, *86*, 3410; *J. Chem. Phys.* **1990**, *92*, 2123 (erratum).
(35) Balasubramanian, K. *Chem. Rev.* **1990**, *90*, 93.
(36) Balasubramanian, K. *J. Mol. Spectrosc.* **1990**, *139*, 405.
(37) Pacios, L. F.; Christiansen, P. A. *J. Chem. Phys.* **1985**, *82*, 2664.
(38) LaJohn, L. A.; Christiansen, P. A.; Ross, R. B.; Atashroo, T.; Ermler, W. C. *J. Chem. Phys.* **1987**, *87*, 2812.
(39) Alekseyev, A. B.; Liebermann, H. −P.; Lingott, R. M.; Bludský, O.; Buenker, R. J. *J. Chem. Phys.* **1998**, *108*, 7695;
(40) Buenker, R. J.; Peyerimhoff, S. D. *Theor. Chim. Acta* **1974**, *35*, 33.
(41) Buenker, R. J.; Peyerimhoff, S. D. *Theor. Chim. Acta* **1975**, *39*, 217.
(42) Buenker, R. J. *Int. J. Quantum Chem.* **1986**, *29*, 435.
(43) Buenker, R. J.; Peyerimhoff, S. D.; Butcher, W. *Mol. Phys.* **1978**, *35*, 771.
(44) Buenker, R. J. In *Proceedings of the Workshop on Quantum Chemistry and Molecular Physics*; Burton, P., Ed.; University Wollongong: Wollongong, Australia; 1980. *Studies in Physical and Theoretical Chemistry*; Carbó, R., Ed.; Current Aspects of Quantum Chemistry 21; Elsevier: Amsterdam, 1981.
(45) Buenker, R. J.; Phillips, R. A. *J. Mol. Struct. (THEOCHEM)* **1985**, *123*, 291.
(46) Davidson, E. R. In *The World of Quantum Chemistry*; Daudel, R., Pullman, B., Eds.; Reidel: Dordrecht, 1974.
(47) Hirsch, G.; Bruna, P. J.; Peyerimhoff, S. D.; Buenker, R. J. *Chem. Phys. Lett.* **1977**, *52*, 442.
(48) Alekseyev, A. B.; Buenker, R. J.; Liebermann, H.-P.; Hirsch, G. *J. Chem. Phys.* **1994**, *100*, 2989 and references therein.
(49) Cooley, J. W. *Math. Comput.* **1961**, *15*, 363.
(50) Moore, C. E. *Atomic Energy Levels*; National Bureau of Standards: Washington, DC, 1971; Vol 3.